

Dependence of coercivity on length ratios in sub-micron Nd₂Fe₁₄B particles with rectangular prism shape

J. Thielsch, D. Suess, L. Schultz, and O. Gutfleisch

Citation: *Journal of Applied Physics* **114**, 223909 (2013); doi: 10.1063/1.4846795

View online: <http://dx.doi.org/10.1063/1.4846795>

View Table of Contents: <http://scitation.aip.org/content/aip/journal/jap/114/22?ver=pdfcov>

Published by the [AIP Publishing](#)

Articles you may be interested in

[Textured Nd₂Fe₁₄B flakes with enhanced coercivity](#)

J. Appl. Phys. **111**, 07A735 (2012); 10.1063/1.3679425

[Comparative study of finite temperature demagnetization in Nd₂Fe₁₄B and SmCo₅ based hard-soft composites](#)

J. Appl. Phys. **110**, 073918 (2011); 10.1063/1.3646474

[Anisotropic Nd₂Fe₁₄B nanoparticles and nanoflakes by surfactant-assisted ball milling](#)

J. Appl. Phys. **109**, 07A759 (2011); 10.1063/1.3567049

[Tb nanoparticles doped Nd–Fe–B sintered permanent magnet with enhanced coercivity](#)

Appl. Phys. Lett. **94**, 092501 (2009); 10.1063/1.3093818

[Microstructure and exchange coupling in nanocrystalline Nd₂\(Fe, Co\)₁₄B–Fe Co particles produced by spark erosion](#)

Appl. Phys. Lett. **86**, 122507 (2005); 10.1063/1.1890474



AIP | **Journal of
Applied Physics**



Journal of Applied Physics is pleased to
announce **André Anders** as its new Editor-in-Chief

Dependence of coercivity on length ratios in sub-micron Nd₂Fe₁₄B particles with rectangular prism shape

J. Thielsch,^{1,a)} D. Suess,² L. Schultz,^{1,3} and O. Gutfleisch^{4,5}

¹Institute for Metallic Materials, IFW Dresden, Dresden D-01171, Germany

²Christian Doppler Laboratory, Institute for Solid State Physics, University of Technology, Vienna A-1040, Austria

³Institute for Material Science, Dresden University of Technology, Dresden D-01069, Germany

⁴Materialwissenschaft, Technische Universität Darmstadt, Darmstadt D-64287, Germany

⁵Fraunhofer Project Group Material Recycling and Resource Strategies IWKS, Alzenau D-63755, Germany

(Received 15 October 2013; accepted 27 November 2013; published online 12 December 2013)

Demagnetization curves of sub-micron Nd₂Fe₁₄B particles with rectangular prism shapes were simulated by micromagnetic simulations. Coercivity decreases with increasing particle thickness for same particle volumes. This unexpected behavior can be explained by different resulting angles of the total effective field when superimposing the applied field vector with the stray field vector at the point of the first reversal event. The angular dependence of the nucleation field follows a Stoner-Wohlfarth like behavior. © 2013 AIP Publishing LLC. [http://dx.doi.org/10.1063/1.4846795]

I. INTRODUCTION

Nd₂Fe₁₄B is at present times in terms of the energy density the strongest permanent magnet material known and is indispensable in our everyday life. There are different production routes in order to produce Nd-Fe-B anisotropic magnets. One of them is hot compaction and deformation of melt-spun ribbons. In hot-deformed samples, the grains are mainly platelet shaped with lateral dimensions of approximately 400 nm × 100 nm.^{1,2} These particular magnets exhibit interaction domains^{1–9} which is a collective phenomenon, i.e., each interaction domain encompasses many grains instead of each grain containing many magnetic domains, as in, e.g., sintered magnets. Even though interaction domains have been under investigation, important aspects are not yet understood. Amongst them are the nature of the magnetization reversal process, the character of an interaction domain wall and its energy and the behaviour of the domains when cooling through the spin reorientation transition at 135 K. Here, we focus on the magnetization reversal process of single independent particles and in order to gain further insight we use micromagnetic simulations, which have been also applied in single nanomagnets with different shapes in order to study reversal processes.¹⁰ The here investigated particles are approximated as rectangular prisms and are varied in their length ratios. Results on single independent grains are the first step on the way of understanding the magnetization reversal process of interaction domains. In a next step, we will look into the behaviour of interacting particle assemblies (which is not a subject of the present paper).

II. MODELING

For the micromagnetic simulations the software FEMME was used, which is based on a hybrid finite element/boundary element method.¹¹ An implicit time integration scheme is

used for the solution of the Landau-Lifshitz Gilbert equation. Sub-micron sized Nd₂Fe₁₄B particles were modeled as rectangular prisms with a square base area (Fig. 1) and various heights which result in different demagnetizing factors according to Aharoni.¹²

The base length to height ratios are 4, 8, 16 with the demagnetizing factors being N = 0.65, N = 0.77, and N = 0.86, respectively (Table I). In order to enable comparison, the volume was kept more or less constant and side lengths were adapted to keep the same demagnetizing factors.

For all particles, the following material properties have been taken: exchange length A = 7.7 pJ/m, the magnetocrystalline anisotropy constant K_u = 4.9 MJ/m³, and saturation magnetization M_s = 1281.5 k A/m (J_s = 1.61 T). The resulting exchange length λ_{ex} = (2A/μ₀M_s²)^{1/2} is 2.73 nm. The c-axis, which is the easy axis of magnetization, is oriented along the short side of the particles. Simulations have been performed with an applied magnetic field starting from the saturated state (remanent state), where the magnetization is homogeneously aligned along the c-axis. In order to study the hysteresis loop an external field is applied, which is increased from 0 to 15 T within a time of 20 ns. The field is applied at an angle of 0.5° with respect to the easy axis antiparallel to the initial magnetization, which leads finally to the demagnetization of the particle. Since we are not interested in the detailed dynamics of the system a large damping constant of 1 was assumed. For selected sample shapes, resulting stray field vectors have been recorded throughout the magnetization reversal process. The mesh elements were tetrahedrons with a maximum size of 4 nm which is above the exchange length of the material but reduces significantly memory space. For one particle with the size of 320 × 320 × 40 nm³, three different mesh sizes have been chosen in order to validate the influence on the trend of coercivity investigated here.

III. RESULTS AND DISCUSSION

Figure 2(a) shows demagnetization curves of NdFeB particles with (almost) identical particle volume

^{a)}Author to whom correspondence should be addressed. Electronic mail: j.thielsch@ifw-dresden.de

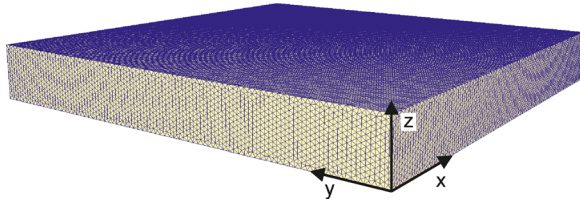


FIG. 1. Example for geometry and mesh of the modeled particle. The shape is a rectangular prism with a square base area.

(about $4 \times 10^6 \text{ nm}^3$) but different demagnetizing factors. Coercivity $\mu_0 H_c$ is 5.68 T, 5.78 T, and 5.96 T for $N = 0.65$, $N = 0.77$, and $N = 0.86$, respectively. Thus, a thinner sample which should lead to a larger internal demagnetization field exhibits a larger coercivity. This behavior is unexpected since a larger internal demagnetization field is expected to support the demagnetization of the body.

Figure 2(b) presents demagnetization curves of a NdFeB particle with the size of $320 \times 320 \times 40 \text{ nm}^3$ and a demagnetization factor of $N = 0.77$, modeled with different mesh sizes. The coercivity $\mu_0 H_c$ is 5.778 T, 5.792 T, and 5.797 T for a mesh size of 4 nm, 3 nm, and 2.5 nm, respectively. With increasing mesh size, the coercivity slightly decreases

TABLE I. Length scales and volume of modeled $\text{Nd}_2\text{Fe}_{14}\text{B}$ rectangular particles with corresponding aspect ratio (height/width) and demagnetizing factor according to Aharoni.¹²

Width/nm	Height/nm	Volume/ 10^6 nm^3	Aspect ratio height/width	Demagnetizing factor N
250.0	62.5	3.906	1:4	0.65
320.0	80.0	8.192		
400.0	100.0	16.000		
320.0	40.0	4.096	1:8	0.77
400.0	50.0	8.000		
504.0	63.0	16.003		
400.0	25.0	4.000	1:16	0.86
504.0	31.5	8.002		
635.2	39.7	16.018		

because of the exchange energy being underestimated when the mesh size is above the exchange length. The difference of 19 mT between the smallest (2.5 nm) and the largest (4 nm) mesh is negligible since the presented change of coercivity for various shapes is by an order of magnitude larger.

For the particle with side lengths of $320 \times 320 \times 40 \text{ nm}^3$, the magnetization states along the hysteresis loop are shown

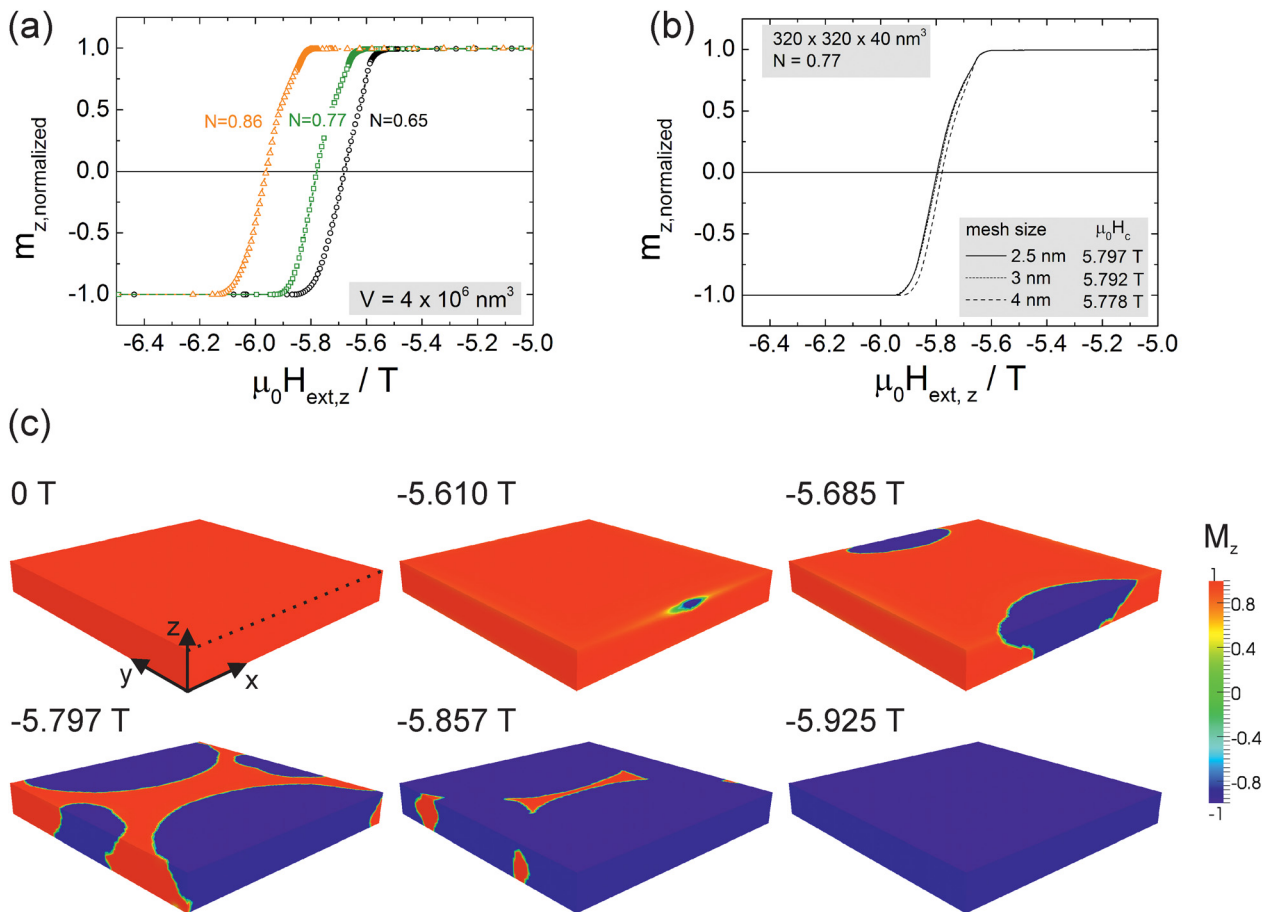


FIG. 2. (a) Demagnetization curve of $\text{Nd}_2\text{Fe}_{14}\text{B}$ particles with identical particle volume but due to different side ratios with different demagnetizing factors N. (b) Demagnetization curves of an $\text{Nd}_2\text{Fe}_{14}\text{B}$ particle with geometry $320 \times 320 \times 40 \text{ nm}^3$ with mesh size of 2.5 nm (below exchange length) as well as 3.0 nm and 4.0 nm (above exchange length). The difference in coercivity resulting from the different mesh sizes is comparably low and does not influence the overall trend investigated here. (c) Images of the magnetization reversal process of a rectangular prism shaped NdFeB particle with side lengths of $320 \times 320 \times 40 \text{ nm}^3$ starting from the saturated/remanent state (upper row, left). The reversal process occurs via nucleation of reversed domains at the edges of the particle and proceeds via domain wall propagation. In the saturated state (last row, right), all magnetic moments are aligned along the direction of the applied field.

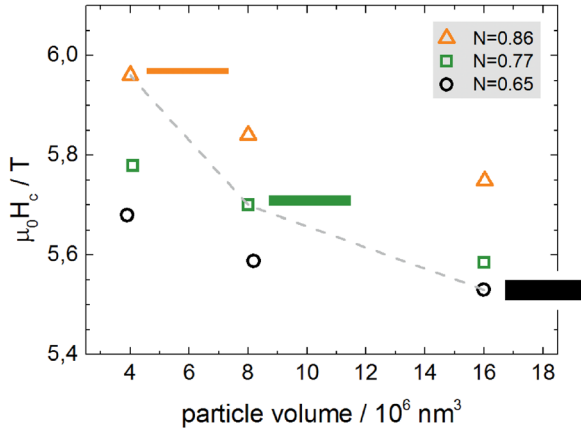


FIG. 3. Coercivity $\mu_0 H_c$ of $\text{Nd}_2\text{Fe}_{14}\text{B}$ particles in dependence of the particle volume for different particle shapes that result in different demagnetizing factors. The volume was kept constant to make direct comparisons feasible. Coercivity $\mu_0 H_c$ is increasing with smaller particle size and also surprisingly with larger demagnetizing factors. The dashed line represents particles with the same basal area ($400 \times 400 \text{ nm}^2$) but different heights (see also sketched cross sections).

in Fig. 2(c). All here presented particles have in common that magnetization reversal proceeds via nucleation of reversed domains and domain wall propagation. Thereby the nucleation always takes place at the edges of the particle. In terms of interaction domains, we can assume that the reversal of a domain in an assembly of interacting grains will also proceed via nucleation and domain wall propagation. That was already predicted from field dependent investigations^{1,2,9} but all methods used are only presenting snapshots. Therefore, simulations help to get an insight.

The trend of coercivity being larger with greater demagnetization factor also appears for particles with a larger volume (up to $16 \times 10^6 \text{ nm}^3$) as can be seen in Figure 3.

In order to understand why an increased demagnetization factor does not necessarily favor the demagnetization, we need to gain information about the total effective field acting, especially at the point of the first reversal event. Therefore, the stray field vectors were recorded from the starting state until the first magnetic spins switch into

the direction of the applied field. In the following discussion, we focus on the particles having the same basal area of $400 \times 400 \text{ nm}^2$ but different heights (dashed line in Figure 3).

Figure 4 presents (a) the magnitude of the stray field vector and (b) the off-axis angle of the stray field vector towards the negative z-axis along the edge of the particles where the first nucleation event occurs. All values shown in this figure were taken at the initial state (zero field—all magnetic moments are pointing along positive z-axis).

Results show that the magnitude of the stray field vectors differs for the various particle geometries. While the shape of the curves are for all particles very similar, with the lowest values at the corners and the maximum values in the middle of the particle edge, the magnitude is highest for the thickest particle. Additionally, we see in Figure 4(b) that with increasing sample thickness the stray field vector exhibits a larger off-axis angle towards the negative z-axis. That means that the vector is more tilted towards the magnetic hard axis which would lead to a larger torque acting on the magnetization. In all three cases, the position of the first nucleation occurrence is more or less in the middle of the edge (Fig. 2(c)) and marked with a symbol. For this point of first reversal, the evolution of both vector parameters with increasing applied field is presented in Figure 5.

The vector magnitude decreases smoothly and drops sharply before reaching the switching/reversal field at this point. For the sample with $N = 0.86$, a larger external field is necessary to trigger nucleation compared to the other ones. The off-axis angle is rather constant throughout the major part of the field range and changes only before nucleation starts (Figure 5). It is obvious that the largest sample ($N = 0.65$) shows stronger deviations when coming close to the switching/reversal field.

For elements with similar shape, it was shown by Dittrich *et al.*¹³ that the angle dependence of the switching field shows a Stoner-Wohlfarth-like behavior even when magnetization reversal proceeds via nucleation and wall propagation. That was explained by the angle dependence of the critical nucleation field that is necessary to create a reversed domain.¹⁴

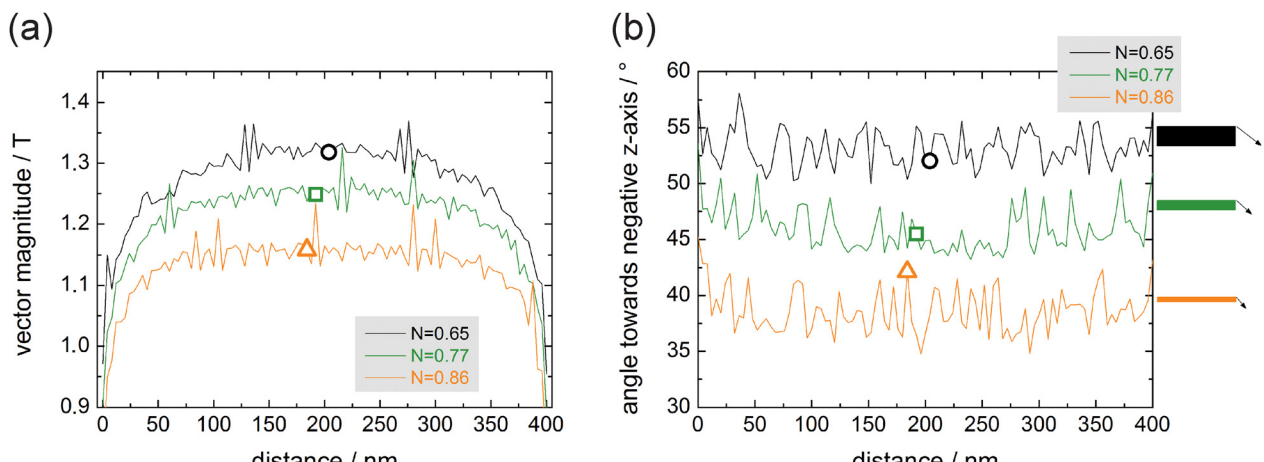


FIG. 4. (a) Magnitude of stray field vector and (b) off-axis angle towards negative z-axis along the edge length (parallel to the x-axis) of the particle where the first reversal event occurs—dashed line in Fig. 2(c). The symbols mark the point of the first reversal event.

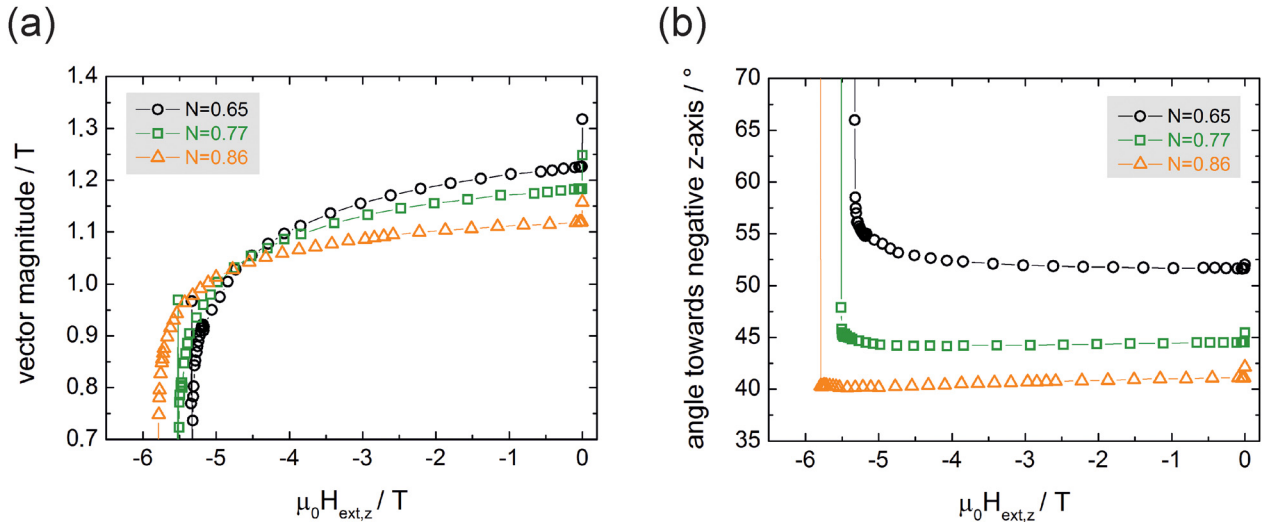


FIG. 5. (a) Magnitude of stray field vector and (b) off-axis angle towards negative z-axis in dependence of an applied field (antiparallel to magnetization) at the point of the first reversal event.

In the case of the here presented elements, we selected the weakest point, where nucleation occurs the first time to evaluate the critical field for nucleation by using the equation of Stoner and Wohlfarth for inverse applied fields at an angle to the direction of M_r ,¹⁵

$$H_R(\psi) = H_A (\sin^{2/3}\psi + \cos^{2/3}\psi)^{-3/2}, \quad (1)$$

with H_A being the anisotropy field ($H_A = 2\mu_0 K_1/J_s$), H_R the reversal field at which the magnetization reversal process sets in and ψ the angle of the total effective field H_{total} . This total effective field is the superposition of the applied external field H_{appl} and the stray field H_{stray} (sketch in Figure 7) and is treated as the “tilted applied field.” The further procedure was as follows: The applied magnetic field H_{appl} was gradually increased in z-direction and for every single field value of H_{appl} the corresponding stray field vector H_{stray} was taken from the micromagnetic simulations to obtain the total field vector $H_{\text{total}}(\psi)$ and the resultant angle ψ .

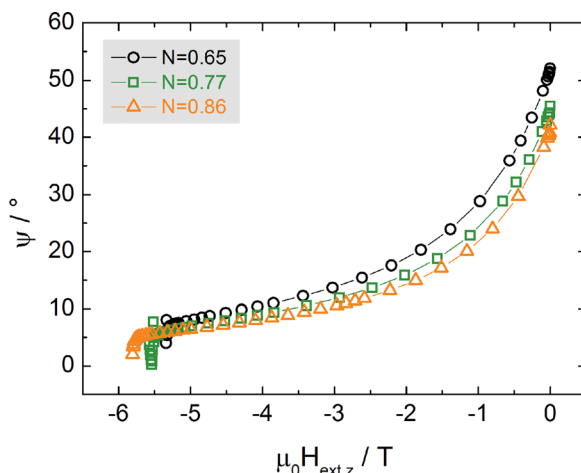


FIG. 6. Angle ψ of the total field vector H_{total} in dependence of the applied magnetic field $H_{\text{ext},z}$.

This angle ψ is changing drastically with increasing applied magnetic field (Figure 6). That is because the contribution of the applied field compared to H_{stray} is becoming steadily larger when H_{appl} is increased.

The angle ψ is largest for the particle with $N = 0.65$, which results from the stray field vector of this sample, which showed the biggest off-axis angle. In addition for the particle with $N = 0.65$ the stray field at the investigated position is larger than for the other samples, which also contributes to a larger tilt of the angle ψ .

When the total effective field H_{total} is large enough and the angle dependent condition,

$$H_{\text{total}}(\psi) > H_R(\psi) \quad (2)$$

is fulfilled the reversal process starts at the point of investigation.

In Figure 7, the corresponding field values when $H_{\text{total}}(\psi) = H_R(\psi)$ is satisfied are shown.

The calculated reversal field H_R shows the same trend as the micromagnetically obtained H_c values, which is the consequence of the different angles ψ for the different geometries. H_R is for all particles smaller than the coercive field which is plausible since H_R was only calculated for one specific magnetic spin—namely the one that is reversing at first. In contrast to that H_c presents the situation when the net

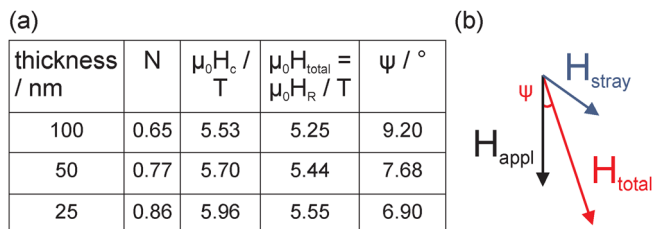


FIG. 7. (a) Table with $\mu_0 H_c$ (obtained by the micromagnetic simulations), $\mu_0 H_{\text{total}}$, $\mu_0 H_R$, and ψ for different particle thicknesses and N when condition $H_{\text{total}}(\psi) = H_R(\psi)$ is first fulfilled. (b) Sketch of the superposition of the stray field H_{stray} and applied magnetic field vector H_{appl} to obtain the total effective field vector H_{total} and ψ .

moment of all magnetic spins becomes zero and therefore more spins have to be reversed into the direction of the applied field.

Nucleation of reversed domains is known to be dependent on the angle of the applied field.^{13,14} Here, the applied field is parallel to the easy axis of the particle. However, since it is superimposed with the acting stray field (which is generated by the magnetic body itself) it results in a total effective field H_{total} , which significantly deviates from the easy axis. The results validate a Stoner-Wohlfarth-like behavior in the investigated samples. The here presented study makes clear that not only the internal demagnetization field (depending on the demagnetizing factor) is important for magnetization reversal processes but more important the total effective field at the position of the first nucleation event. So it comes that a magnetic body with a larger internal demagnetizing field can exhibit a higher coercive field.

IV. CONCLUSION

It was shown that the coercive field of the hard magnetic particles with the shape of rectangular prism can be understood by investigating the strength and the angle of the total effective field at the point of the first reversal (nucleation) using the Stoner Wohlfarth theory. The angle of the total field at the point of the nucleation results from the superposition of an applied field being parallel to the easy axis and the stray field generated by the magnetic particle itself. A larger angle leads to a faster magnetization reversal which can be explained by a larger torque acting on the magnetization. The consequence is the counterintuitive effect that the particles with the largest demagnetization fields are the hardest to demagnetize.

In terms of the interaction domains, we can assume that the reversal of a domain in an assembly of interacting grains will also proceed via nucleation and domain wall propagation. That was already predicted from field dependent

investigations^{1,2,9} but since all methods are only presenting snapshots of the reversal process simulations help to make it a sound prediction.

ACKNOWLEDGMENTS

The authors are thankful to K.-H. Müller and T. G. Woodcock for helpful discussions. D.S. acknowledges the financial support from the Austrian Federal Ministry of Economy, Family and Youth and the National Foundation for Research, Technology and Development as well as the Austrian Science Fund FWF, Project SFB-ViCoM, F4112-N13.

- ¹J. Thielsch, D. Hinz, L. Schultz, and O. Gutfleisch, *J. Magn. Magn. Mater.* **322**, 3208 (2010).
- ²J. Thielsch, H. Stopfel, U. Wolff, V. Neu, T. G. Woodcock, K. Güth, L. Schultz, and O. Gutfleisch, *J. Appl. Phys.* **111**, 103901 (2012).
- ³D. C. Crew, L. H. Lewis, and V. Panchanathan, *J. Magn. Magn. Mater.* **231**, 57 (2001).
- ⁴L. Folks, R. Street, and R. C. Woodward, *Appl. Phys. Lett.* **65**, 910 (1994).
- ⁵L. Folks, R. Street, R. C. Woodward, and K. Babcock, *J. Magn. Magn. Mater.* **159**, 109 (1996).
- ⁶K. Khlopkov, O. Gutfleisch, R. Schäfer, D. Hinz, K.-H. Müller, and L. Schultz, *J. Magn. Magn. Mater.* **272**, E1937 (2004).
- ⁷K. Khlopkov, O. Gutfleisch, D. Hinz, K.-H. Müller, and L. Schultz, *J. Appl. Phys.* **102**, 023912 (2007).
- ⁸V. V. Volkov and Y. Zhu, *J. Appl. Phys.* **85**, 3254 (1999).
- ⁹V. V. Volkov and Y. Zhu, *J. Magn. Magn. Mater.* **214**, 204 (2000).
- ¹⁰P. Krone, D. Makarov, M. Albrecht, T. Schrefl, and D. Suess, *J. Magn. Magn. Mater.* **322**, 3771 (2010).
- ¹¹D. Suess, V. Tsiantos, T. Schrefl, J. Fidler, W. Scholz, H. Forster, R. Dittrich, and J. Miles, *J. Magn. Magn. Mater.* **248**, 298 (2002).
- ¹²A. Aharoni, *J. Appl. Phys.* **83**, 3432 (1998).
- ¹³R. Dittrich, G. H. Hu, T. Schrefl, T. Thomson, D. Suess, B. D. Terris, and J. Fidler, *J. Appl. Phys.* **97**, 10J705 (2005).
- ¹⁴H. Kronmüller, K.-D. Durst, and G. Martinek, *J. Magn. Magn. Mater.* **69**, 149 (1987).
- ¹⁵E. C. Stoner and E. P. Wohlfarth, *Philos. Trans. R. Soc. London, Ser. A* **240**, 599 (1948).